Synthesis of SnO_2 nanoparticles using plant leaf extract and study of dielectric property of SnO_2 - PPY nanocomposites

Kousik Dutta*
Assistant Professor in Physics
Department of Physics, Behala College, Parnashree; Kolkata- 700060; INDIA
Author for correspondence: duttakousik2003@yahoo.co.in

Abstract : ***Incorporation of biosynthesis technique into nanotechnology is a significant step in nanoscience research because this green protocol of synthesizing nanoparticles is cost effective, quite safe and eco-friendly compared to the conventional chemical and physical methods. For these reasons, in recent years, this green and bio-based route for the preparation of nanoparticles has gained much attention, and many metal and metal oxide nanoparticles have been prepared by using this method in which plant source, bacteria, fungus and some biological materials are used. In this paper it is reported that the biosynthesis of Tin Oxide nanoparticles (SnO_2-NPs) using guava leaf exact. Inorganic-organic hybrid nanocomposites are synthesized by dispersing nanosized SnO_2 in the conducting polypyrrole matrix. The morphology of crystalline phase of nanocomposite was determined from Scanning Electron Microscopy (SEM), transmission electron microscopes (TEM) and X-ray diffraction (XRD) spectra. The average size of SnO_2 nanoparticles was in the range of 15 nm and the observed morphology was spherical. Complex impedance and dielectric permittivity of SnO_2-PPY nanocomposite have been investigated as a function of frequency and temperature at different compositions. The dielectric permittivity 3800 is observed. Large value of permittivity is well described by Maxwell-Wagner polarization. Broad and asymmetric dielectric spectra are analyzed by Harviliak - Nigami relaxation function.***

Key words: Green Synthesis, SnO_2 nanoparticles, SnO_2-PPY nanocomposites, dielectric properties

I. INTRODUCTION

Nanoscale oxide semiconductors have been studied enormously for their distinctive optical, electronic, magnetic, catalytic and medicinal properties as compared with the traditional and commercial bulk materials [**1-3**]. These unique properties generated researchers interest in the synthesis of nanoscale materials with different sizes, shapes, and compositions. For this purpose, during the last two decades, a vast number of physical and chemical synthetic routes have been established. In recent years, for reducing or removing the use of toxic chemicals, the comparatively new and largely unexplored bio-mediated green synthesis technique has been developed. This biogenic synthesis of nanoparticles depends on the source materials [**4**] such as plants and plant parts, bacteria, fungus and other bio-based molecules (protein, vitamin, molecules etc.) used in the procedure. The plant phytochemicals which have antioxidant property is mainly responsible for the preparation of metal and metal oxide nanoparticle. Besides, many biological components have abilities to act as templates in the synthesis and help to produce a self assembled nanoscale material. So a novel and economically beneficial bio-based green synthesis method may be a better alternative choice for the synthesis of metal oxide nanoparticles compared to commonly used chemical and physical methods.

Among the semiconducting nanoparticles, Tin oxide (SnO_2) has been studied intensely because of its potential applicability to lithium-ion batteries [**5**], transparent conducting electrodes in ionic devices [**6**], anti-reflective coatings [**7**], solid-state gas sensors [**8**], solar cells [**9**], energy storage [**10**] etc. A large number of physical and chemical methods have already been reported in the literature to fabricate different types of SnO_2 nanostructures such as hydrothermal method [**11**], solvothermal [**12**], co precipitation method [**13**], sol-gel [**14**], chemical vapor deposition [**15**] etc. However, due to many disadvantages of these routes like toxicity of the chemicals, expensive equipment, energy waste and environmental pollution developing facile and green methods for synthesizing tin oxide nanoparticles has drawn much importance in the recent years

researchers due to their simplicity and eco friendly approach. It is cost effective and therefore can be used as an economic and viable alternative for the large scale production of metal oxide nanoparticles.

The rate of nano synthesis or the stability of the product depends on the reducing agents, capping agents used during the synthesis of nanomaterials. But in the green synthesis of nanomaterials, the alkaloids, flavones, terpenes, amino acids and carbohydrates present in the plant materials act as the reducing agents and capping agents which plays a major role on the surface morphology and size of the metals. Numerous approaches have been used to synthesize nanoparticles and toxic chemicals that are used in physical and chemical methods may reside in the nanoparticles formed which may prove hazardous to the environment and organisms in the field of their application [**16**]. In recent years, the synthesis of nanoparticles using green approach has been increased. Green synthesis is an efficient technique which includes synthesis through plants, bacteria, fungi, algae, actinomycetes etc. Green approach is an environment friendly, cost effective, biocompatible and safe . Nanoparticles synthesized from this approach produce more catalytic activity and limit the use of expensive and toxic chemicals. The present study is endeavored to use green approach to synthesize Tin oxide nanoparticles using Psidium Guajava (guava) leaf extract by a simple and economical synthesis method. Guava leaf extracts have found to contain phenolic compounds, flavonoids, sesquiterpene alcohols and triterpenoid acids which possess antioxidant, antimicrobial as well as antitumor properties.

TABLE I: Weight percentage of pyrrole (x), real part of relative dielectric permittivity (ϵ_1) at room temperature (RT)

Sample	x	ϵ1(RT)
S1	20	3800
S2	35	3200
S3	50	2600
S4	65	2100

Polypyrrole (PPY) is one of the most studied conducting polymers because of its good electrical conductivity, environmental stability and relatively easy synthesis [**17-18**]. Monomers are polymerized in the aqueous solution in the presence of metal and oxide nanoparticles to obtain nanocomposites. The composites of polypyrrole with gold nanoparticles and different kinds of inorganic oxides such as NiO, SnO_2, CuO, ZnO, CeO_2, etc [**19 - 20**] have been synthesized by various chemical routes. Colloidal dispersion of inorganic nanoparticles within the polymer matrix, as suggested by Han and Armes, is a very efficient and novel chemical process to prepare homogeneous Composites [**21**]. In the present paper, it is reported that SnO_2 nanoparticles are synthesized using guava leaf extract and then these nanoparticles are embedded in conducting PPY to prepare SnO_2-ppy nanocomposite. Observation of the temperature and frequency dependence of dielectric properties for SnO_2-PPY nanocomposite is the major aim of this report.

II. MATERIALS AND METHODS

Guava leaves were collected locally. All the chemicals were of analytical grade and purchased from Merck (India) and used without further purification. Pyrrole (AR grade) was purified and stored at -15^{0}C in a refrigerator prior to use. APS oxidant was used as received and de-ionized water was employed for preparing all the solutions and reagents. The samples were characterized by x-ray powder diffraction patterns employing a scanning rate of 0.02 0 per 2 sec in 2θ range from 20 to 70 using a Philips (PW1710) x-ray diffractometer equipped with monochromatized Cukα radiations. The nanocrystalline powder was pressed inside the sample holder and X-ray data were collected in step scan mode. Morphological studies were performed with JEOL JSM6700F Scanning electron microscope (SEM). Transmission electron micrograph (TEM) was taken from JEOL, JEM 2010 with acceleration voltage of 200 KV. FTIR spectrometer were recorded as Kerr disc on PerkinElmer Spectrum-2000, FTIR spectrophotometer between 500 and 4000 cm^{-1} . The temperature dependent capacitance (C) and dielectric loss factor (D) were measured by Agilent 4192 Impedance Analyzer. The electrical contacts were made by silver paint on both sides of the sample. Dry powdered sample were made into pellets using a steel die of 1 cm diameter in a hydraulic press under a pressure of 7 ton. The thickness of the samples varies from 0.05 cm to 0.10 cm. For electrical measurements

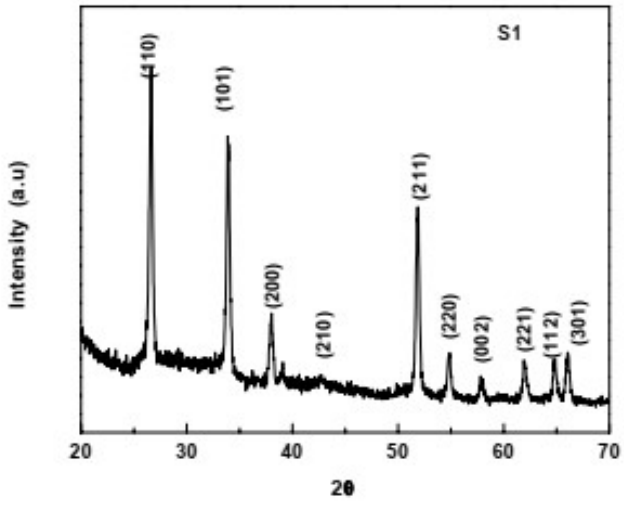

Figure 1: X-ray diffraction pattern of SnO_2 - PPY nanocomposite sample S1.

A. Preparation of guava leaf extract

The as-collected guava leaves were first cleaned and washed to remove dust particles and placed under sunlight. The dried leaves were grinded and dissolved in 500 ml water with continuous stirring and heating at 80°C for 3hrs. The brownish extract was obtained by filtering the as-treated material using filter paper.

B. Synthesis of Tin Oxide (SnO_2) nanoparticles by Guava leaf extract

SnO_2 nanoparticles production was done by biosynthesis using guava plant leaf extract as stabilizing/capping agent. For this about 2.1 M $SnCl_4$ was added drop wise to guava leaf extracts in the ratio 1:1 (w/w %) and stirred for 3.5 hrs at 80°C. After 3.5 hrs, the stirring was continued at room temperature until the mixture was transformed to jelly form which was then calcined at 500°C for 6 hrs to obtain SnO_2 NPs. Powder was obtained and this was carefully collected and dried in a vacuum oven for 60ºC for 2 hours.

C. Synthesis of SnO_2-PPY nanocomposite

The required quantity of SnO_2 nanoparticle was ultrasonically dispersed in 40 ml deionized water. Pyrrole monomer of known volume was slowly added into the dispersion under sonication at room temperature. Then the aqueous solution of APS maintaining a pyrrole : APS mole ratio of 1:1.25 was added drop wise into the previous solution. After few hours the resulting solution was turned into black color which indicates the formation of polypyrrole. The solution was then kept under sonication for about 12 hours to ensure complete polymerization. Finally the resulting black dispersion were centrifuged. The resulting nanocomposites were washed thoroughly with distilled water for several times. Different compositions of nanocomposite samples by varying the weight percentage of pyrrole (polypyrrole) were prepared as shown in Table I.

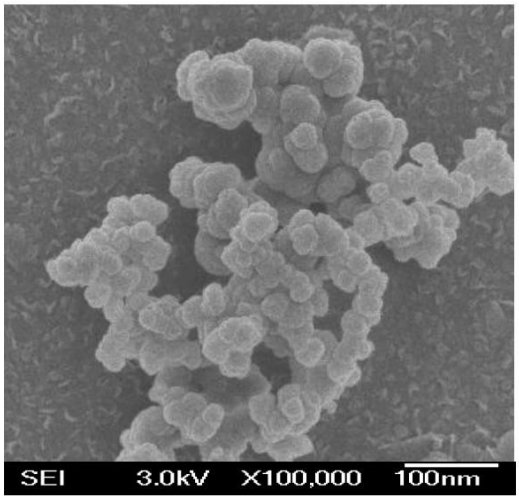

Figure 2: Scanning electron micrograph of sample S1.

III. RESULTS AND DISCUSSION

Fig 1 shows the characteristic peaks of X-ray diffraction (XRD) of the sample S1. All the diffraction lines are assign to tetragonal rutile crystalline phase of tin oxide which indicates the presence of SnO_2 in the nanocomposite. The XRD pattern is an excellent agreement with a reference pattern (Powder diffraction file no -21-1250) of the tin oxide.

The scanning electron micrograph (SEM) of the nanocomposite sample S1 is shown in Figure 2. The SnO_2 nanoparticles are well dispersed and are of spherical in shape with uniform diameter lying in the range from 25- 30 nm. Larger particle size may be due to the aggregation of smaller particles in the presence of polymer matrix.

Figure 3. shows the TEM micrograph of the SnO_2 - polypyrrole nanocomposite S1 sample. In this micrograph nearly, spherical crystallites are observed. The mean particle size of pure SnO_2 is in the range of 15-20 nm which is good agreement with XRD result. Larger particle size due to the aggregation of smaller particles in the presence of polymer matrix having particle size in the range 30-35 nm.

Fig. 4 shows FTIR spectra of the nanocomposite sample S1. The band at 1552 cm^{-1} corresponds to typical pyrrole rings vibration. The peak at 1467 cm^{-1} is attributed to = CH in plane vibration and peaks at 921 cm^{-1} and 793 cm^{-1} due to =CH out of plane vibration. The characteristic bands at 1310 cm^{-1}, 1190 cm^{-1}, 1050 $cm^{-1}$and 664 $cm^{-1}$are related to C-H and N-H in-plane and bending vibrations. In the low wave number region a strong vibration around 613 cm^{-1} is observed which corresponds to antisymmetric Sn-O-Sn mode of the tin oxide. Almost all the bands reveal blue shift in the nanocomposites which indicates that there is a strong interaction between polypyrrole and SnO_2 nanoparticles.

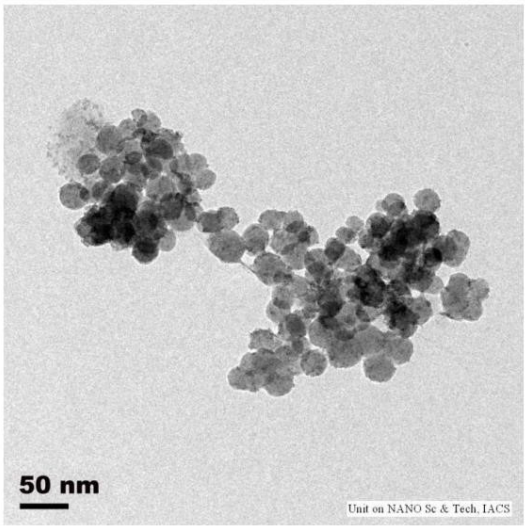

Figure 3: Tunneling electron micrograph of sample S1.

Fig. 5 represents the complex impedance, $Z=Z_1 +iZ_2$ plots for the sample S1 at different temperatures. The addition of SnO_2 nanoparticles in the PPY matrix gives rise to two incomplete semicircles.

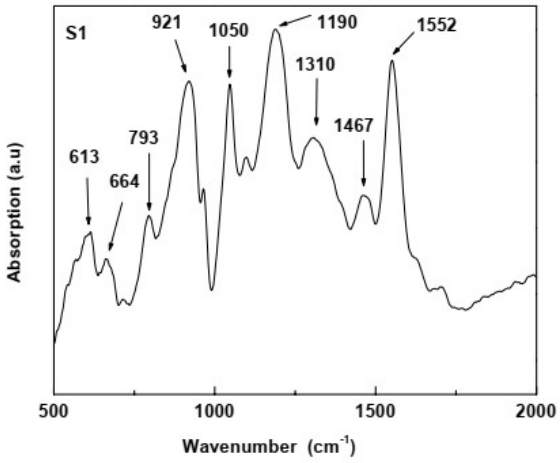

Figure 4: Fourier transform infrared (FTIR) spectra of sample S1.

The high frequency contribution dominates with lowering of temperature. The features of the impedance spectra of polycrystalline composite materials primarily depend on the microstructure. The nanocomposites consist of nanometer size grains which introduce more grain boundaries within the samples. The impedance spectra can be interpreted by the equivalent circuit consisting of series connected parallel resistance (R) and capacitance (C) components as shown in Fig. 5. The position of the maximum arc in the impedance diagram is determined by the relation $\omega_{max}RC = 1$, where $\omega_{max} = 2\pi f$, f is the applied frequency.

The larger values of R and C at grain boundary lead to smaller ω_{max} compared to grain. Moreover, ω_{max} lies outside the available frequency range and only some portions of semicircles are obtained at higher temperature. Conducting PPY is adsorbed on the surfaces of SnO_2 nanoparticles. The interface between PPY and SnO_2 is formed. In reality, spectra should exhibit three semicircles associated with grain boundary, grain and SnO_2-PPY interface effects. The grain and grain boundary responses are analyzed by the following relations

$$Z_1 = \frac{R_g}{1+(\omega R_g C_g)^2} + \frac{R_{gb}}{1+(\omega R_{gb} C_{gb})^2}$$

$$Z = R\left[\quad \omega R_g C_g \quad\right] + R\left[\quad \omega R_{gb} C_{gb} \quad\right]$$

where (R_g, R_{gb}) and (C_g, C_{gb}) are resistance and capacitance of grain and grain boundary respectively. Eqs. 1 and 2 represent two ideal semicircles whose centers lie on the real Z_1 axis. The constant phase elements (CPE) capacitors $C(\omega) = B(i\omega)^{n-1}$ are assumed to analyze the more flattened semicircles [**22-23**]. The parameter B is constant for a given set of experimental data. The exponent n varies between 0 and 1. The impedance of CPE behaves as an ideal capacitor for n = 1 and ideal resistor for n = 0. The solid lines in Fig. 5 represent the best fitted calculated values. The value of single C is 3.5 x 10^{-10} F for PPY while it is 3 - 1 x 10^{-11} F (grain) and 0.4-5 x 10^{-8} F (grain boundary). Both C_{gb} and C_g are weak temperature dependent.

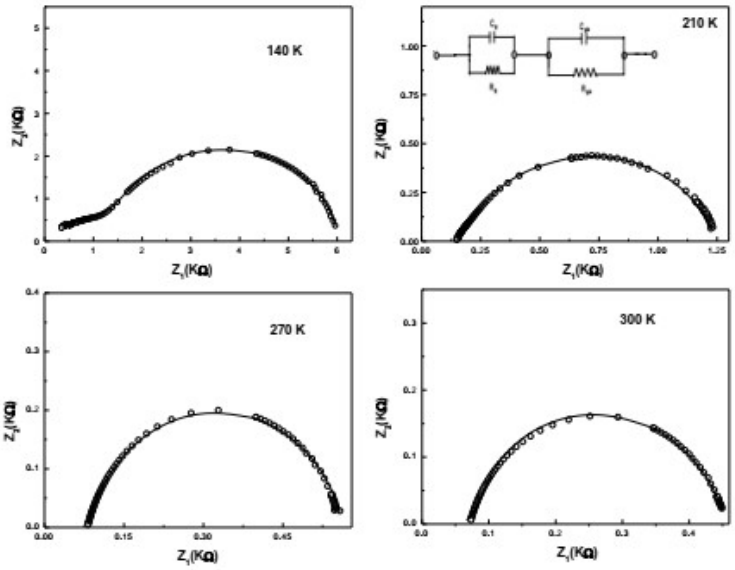

Figure 5: Impedance spectra of the sample S1 at four different temperatures. The solid lines are fits to the proposed equivalent circuit for the sample.

Grain (σ_g) and grain boundary (σ_{gb}) conductivities have been calculated from the best fitted values of R *g* and R_{gb}. For simplicity, the evaluation of σ_g was performed from the relation, $\sigma_g = d/(AR_g)$, where d and A represent thickness and area of pellet sample respectively and similar calculation for σ_{gb}. The estimated grain boundary conductivity is about 12 times lower than that of grain conductivity. Both σ_g and σ_{gb} follow Arrhenius type process with temperature. The activation energy of the grain interioris smaller than that of grain boundary. The conductivity of grain boundary regions mainly determined by the microstructure.

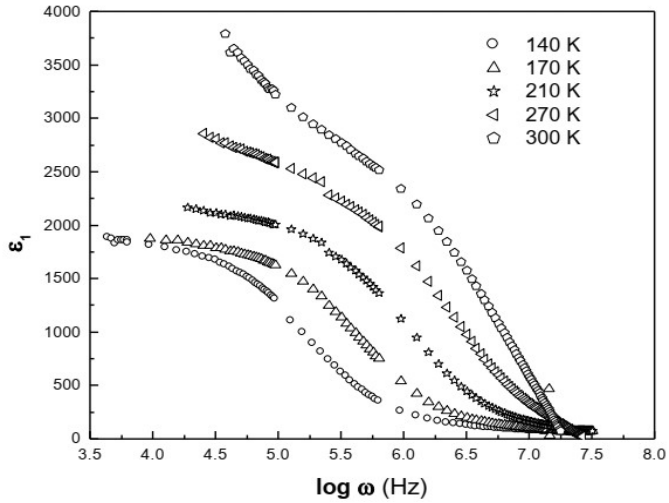

Figure 6: Frequency dependence of the real part of relative dielectric constant (ε_1) at different temperatures for the sample S1.

The dielectric constant ε_1 as a function of frequency at room temperature for sample S1 are shown in Fig. 6.

TABLE I: Davidson-Cole (DC) function best fitted parameters τ and β in Eq. 3 for dielectric loss spectra of sample S1

Temperature (K)	τ(10^{-6} sec)	β
120	3.18	0.93
140	2.15	0.95
160	1.50	0.98
180	1.20	0.999
200	1.01	1
220	0.86	1
240	0.74	1
270	0.68	1
300	0.51	1

An exceptionally high value of about 3800 is found for S1 and has a strong frequency dependency at lower frequency region. The value of ε_1 decreases with decrease of SnO_2 content. At high frequency greater than 1 MHz, ε_1 reaches to about 50 - 100. Low and high frequency dielectric constants are quite large compared to static ε_1 (0) = 3.91 and high frequency ε_1 (∞) = 12.19 of pure tin dioxide. [**24**] Fig. 6. represents the temperature dependence of ε_1 for S1. The step like transition to lower values shifts to lower frequency with decreasing temperature. The high frequency value of ε_1 is almost independent of temperature.

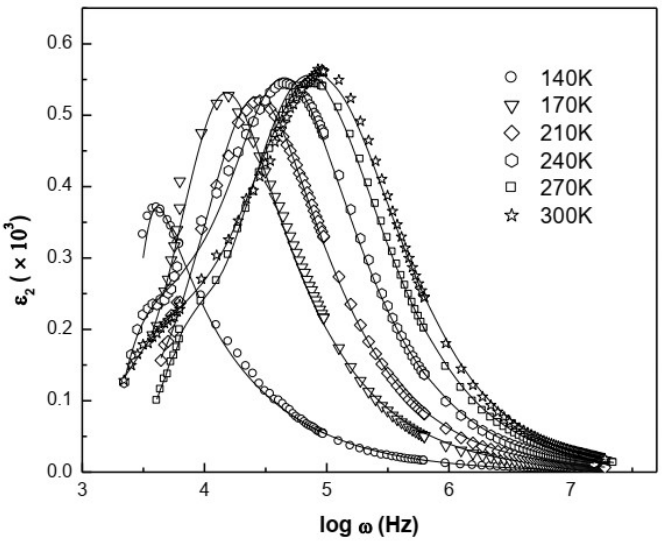

Figure 7: Frequency dependence of imaginary component of dielectric constant (ε_2) at selected temperatures for the sample S1. The solid lines are fits to Eq. 4.

The unusually large dielectric constant can be explained by interfacial Maxwell Wagner (MW) interfacial relaxation commonly applied in heterogenous system. The nanocomposites consist of conducting grains and resistive grain boundaries. Under the application of external electric field, the charge carriers can easily migrate the grains but are accumulated at the grain boundaries. This process can produce large polarisation and high dielectric constant. The small conductivity of grain boundary contributes to high value of dielectric constant at low frequency. The static dielectric constant based on the equivalent circuit in Fig. 5 can be expressed as

$$\epsilon_1(0) = \frac{R_g^2 C_g + R_{gb}^2 C_{gb}}{C_0 (R_g + R_{gb})^2} \quad (3)$$

Resistance and capacitance of grain boundary are much larger than that of grain. In MW polarisation, dielectric constant under such condition can be approximated from Eq. 3 as $\boldsymbol{\varepsilon_1}$ (0) = C_{gb}/C_0. A large value of C_{gb} leads to very high value of dielectric constant. The ratio of SnO_2 and PPY modifies the microstructure i.e. grain boundary capacitance. This may be the possible reason for different values of $\boldsymbol{\varepsilon_1}$ for different compositions.

The dielectric loss spectra $\boldsymbol{\varepsilon_2}$ as a function of frequency for S1 are shown in Fig. 7 for different temperatures. Two relaxation peaks in the measured frequency domain are appeared at low temperature. The positions of the peaks move to lower frequency with the decrease of temperature. The dielectric response has been analyzed by the most generalized Havriliak-Negami (HN) function [**25**].

$$\epsilon^* = \sum_{\delta} [\epsilon_\infty + \frac{\epsilon_s - \epsilon_\infty}{(1 + (i\omega\tau)^\beta)^\alpha}]_\delta \quad (4)$$

where γ corresponds to different relaxation process, τ is the average relaxation time which is given at the frequency of maximum dielectric loss. The difference $\Delta\ \boldsymbol{\varepsilon} = \boldsymbol{\varepsilon}_s - \boldsymbol{\varepsilon}_\infty$ is known as the dielectric relaxation strength. The parameter β describes the distribution of the relaxation time of the system. Debye relaxation is obtained for $\alpha = 1$ and $\beta = 1$. The parameters α and β ranging between 0 and 1 are symmetric and asymmetric broadening of dielectric spectra. The solid lines in Fig. 7 show that the experimental data are reasonably good fitted with the calculated value of HN function. The best fitted curves are obtained for $\alpha = 1$; $\beta = 0.30$ - 0.8 (peak I) and $\alpha = 1$; $\beta = 0.58$ - 0.94 (peak II) .The value of β is different from unity which implies non Debye relaxation process. This parameter manifests that the dielectric dispersion has a broad distribution of relaxation time. The dielectric strength $\Delta\varepsilon$ increases with increase of temperature.

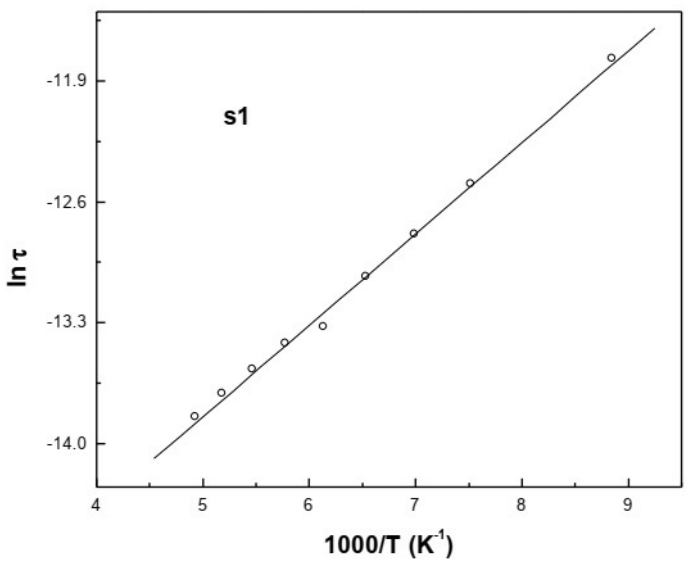

FIG. 8: Arrhenius plot of dielectric relaxation time vs frequency at different temperatures for the sample S1

The relaxation times, τ at different temperatures are obtained from the best fitted data to eqn.5. The Arrehenius plot (not shown in this manuscript) of ln τ against 1/T for the different samples suggest that the temperature variation of τ can be described by thermally activated Arrhenius law,

where τ_0 is the relaxation time at high temperature, E_τ is the activation energy of dielectric process and k is Boltzmann constant. The dielectric constant increases with the volume fraction of SnO_2. Moreover, two dielectric relaxation peaks are only found and within the measured frequency range for the highest content of SnO_2. All these observations suggest that SnO_2 contribute predominantly to the dielectric response. Photoemission experiment [**26**] and the microscopic studies [**27**] show that tin ions in Sn2+ oxidation state exist at the surface. First principles density functional calculations establish that the oxygen deficient surfaces of SnO_2 behave as SnO. [**28**] Oxygen vacancies and the existence of mixed valence state of Sn (Sn4+, Sn2+) produce local lattice distortion in nanosized SnO_2. [**29**] The lattice distortions generate several potential minima. Dielectric relaxation at high frequency may be ascribed to thermally activated motion of charges among the potential minima. The observed activation energy of dielectric relaxation is consistent with the shallow levels associated with intrinsic defects within SnO_2.

IV. CONCLUSION

Impedance data demonstrate the existence of electrically semiconducting grains and more resistive grain boundaries. The values of dielectric constant exhibit large variations with compositions, temperature and frequency. The dielectric response at the lower frequency is characterized by Maxwell-Wagner relaxation and that at higher frequency is attributed to oxygen vacancies of SnO_2.

V. REFERENCES

[1] Sagadevan S., *J. Nanomater. Mol. Nanotechnol.* 4 (2015) 889-894.

[2] Raveendran P., Fu J., Wallen S. L., *J. Am. Chem. Soc.* 125 (2003) 13940-13941.

[3] Li L., Hu J., Yang W., Alivistos A. P., *Nano Lett.* 1 (2001) 349-351.

[4] Castro L., Blázquez M. L., Muñoz J. Á., González F. G., Ballester A., *Rev. Adv. Sci. Eng*. 3 (2014) 199-216.

[5] Chen J. S., Lou X. W., *Small* 9 (2013) 1877-1893.

[6] Chopra K. L., Major S., Pandya D. K., *Thin Solid Films* 102 (1983) 1-46.

[7] Minami T., *MRS Bull*. 25 (2000) 38-44.

[8] Moseley P. T., *Meas. Sci. Technol*. 8 (1997) 223-237.

[9] Shang G., Wu J., Huang M., Lin J., Lan Z., Huang Y., Leqing F., *J. Phys. Chem. C* 116 (2012) 20140-20145.

[10] Kalubarme R. S., Lee J. Y., Park C. J., *ACS Appl. Mater. Interfaces*, 7 (2015) 17226-37.

[11] Patil G. E., Kajale D. D., Gaikwad V.B., Jain G.H., *Int. Nano Lett.* 2 (2012) 17 1-5.

[12] He Z. L., Zhou J. Q., *Mod. Res.Catal.* 2 (2013) 13-18.

[13] Agrahari V., Mathpal M. C., Kumar M., Agarwal A., *J. Alloys. Compd.* 622 (2015) 48-53.

[14] Gnanam S., Rajendran V., *J. Sol-Gel Sci. Technol*. 53 (2010) 555-559.

[15] Liu Y., Koep E., Liu M., *Chem. Mater*. 17 (2005) 3997-4000.

[16] G. Singh, P.K. Babele, A. Kumar, A. Srivastava, R.P. Sinha, M.B. Tyagi, Journal of photochemistry and photobiology. B, Biology 138, 55 (2014).

[17] Torillo G, Garnier F, (1999) J. Electroanal. Chem. 135 172

[18] Skothim T. A. Elenbaumer R., Reynolds J. R. (1998) Handbook of conducting polymers, Marcel Dekker, New York,

[19] S. Maeda, S. P. Armes, (1995), Synt. Synt. Metals 73, 151

[20] Huang C. L., Matijevi E., (1995) J. Mater. Res. 10, 1327

[21] M. G. Han and S. P. Armes, (2003), J. Colloid and Interface Sci., 262, 418

[22] J. R. Macdonald, *Impedance Spectroscopy* John Wiley, New York, (1987)

[23] A. K. Jonscher, in *Solids* Chesla Dielectric Group, UK, (1983)

[24] E. Taverner, C. Rayden, S. Warren, A. Gulion, P. Cox, and A. R. G. Esdell, Phys. Rev. B 51, 6833 (1995)

[25] S. Havriliak and S. Negami, Polymer 8, 161 (1967)

[26] J. M. Themlin, R. Sporken, J. Darville, and J. M. Gilles, Phys. Rev. B 42, 11914 (1990) 46

[27] C. L. Pang, S. A. Haycock, H. Raza, P. J. Moller, and G. Thormton, Phys. Rev. B 62, R7775 (2000) 47

[28] M. A. Maki-Jaskari and T. T. Rantala, Phys. Rev. B 65, 245428 (2002)

[29] K. N. Yu, Y. Xiong, Y. Liu, and C. Xiong, Phys. Rev. B 55, 26669 (1997)